2007-12-03

Effects of Water Vapor on the Kinetics of the Methylperoxy Radical Self-reaction and Reaction with Hydroperoxy

Alecia Mower
Brigham Young University - Provo

EFFECTS OF WATER VAPOR ON THE KINETICS OF THE CH_3O_2 SELF-REACTION AND REACTION WITH HO_2

by

Alecia Mower English

A thesis submitted to the faculty of

Brigham Young University

in partial fulfillment of the requirements for the degree of

Master of Science

Department of Chemistry and Biochemistry

Brigham Young University

December 2007

BRIGHAM YOUNG UNIVERSITY

GRADUATE COMMITTEE APPROVAL

of a thesis submitted by

Alecia Mower English

This thesis has been read by each member of the following graduate committee and by majority vote has been found to be satisfactory.

Date	Jaron C. Hansen, Chair
Date	Delbert J. Eatough
Date	Steven R. Goates
Date	Eric T. Sevy

BRIGHAM YOUNG UNIVERSITY

As chair of the candidate's graduate committee, I have read the thesis of Alecia Mower English in its final form and have found that (1) its format, citations, and bibliographical style are consistent and acceptable and fulfill university and department style requirements; (2) its illustrative materials including figures, tables, and charts are in place; and (3) the final manuscript is satisfactory to the graduate committee and is ready for submission to the university library.

Date	Jaron C. Hansen Chair, Graduate Committee

Accepted for the Department

Date	David V. Dearden Graduate Coordinator

Accepted for the College

Date	Thomas W. Sederberg Associate Dean, College of Physical and Mathematical Sciences

ABSTRACT

EFFECTS OF WATER VAPOR ON THE KINETICS OF THE CH_3O_2 SELF-REACTION AND REACTION WITH HO_2

Alecia Mower English

Department of Chemistry and Biochemistry

Master of Science

The gas phase reactions of $CH_3O_2 + CH_3O_2$, $HO_2 + HO_2$, and $CH_3O_2 + HO_2$ in the presence of water vapor have been studied at temperatures between 263 and 303 K using laser flash photolysis coupled with UV time-resolved absorption detection at 220 nm and 260 nm. Water vapor concentration was quantified using tunable diode laser spectroscopy operating in the mid-IR. The HO_2 self-reaction rate constant is significantly enhanced by water vapor, consistent with what others have reported, whereas CH_3O_2 self-reaction and the cross-reaction ($CH_3O_2 + HO_2$) rate constants are nearly unaffected. The enhancement in the HO_2 self-reaction rate coefficient occurs because of the formation of a strongly bound (6.9 kcal mol^{-1}) HO_2-H_2O complex during the reaction mechanism where the H_2O acts as an energy chaperone. The nominal impact of water vapor on the CH_3O_2 self-reaction rate coefficient is consistent with recent high level *ab initio* calculations that predict a weakly bound CH_3O_2-H_2O complex (3.2

kcal mol^{-1}). The smaller binding energy of the CH_3O_2-H_2O complex excludes its formation and consequent participation in the methyl peroxy self-reaction mechanism.

ACKNOWLEDGEMENTS

Acknowledgments. Acknowledgements. I thank my grandparents, Marvin and Ruth Elaine Mower for their encouragement and support to be a graduate student. Thanks to my husband, Justin, for being the kindest person to me and for listening to Marvin when he admonished him to see that I finished school. My siblings and parents are kind enough to listen to the highs and lows of my studies. And thanks go to little Ruth Elaine for hanging out with me in the lab everyday *in utero*.

Joe Szente (Ford Motor Company) has been my mentor and friend with unending knowledge and patience. My BYU advisor, Jaron Hansen, has provided me with many opportunities and made my degree possible. I thank both of them for their faith in me. I thank Matti Maricq (Ford Motor Company) for his astute ideas and kind words. Thanks to Ford Motor Company for allowing me a place to do this research.

Lastly, thanks go to H_2O for always finding new ways to be interesting.

TABLE OF CONTENTS

LIST OF TABLES

LIST OF FIGURES

CHAPTER 1: INTRODUCTION

1.1 Peroxy Radicals

1.1.1 Role of Peroxy Radicals

Peroxy radicals (RO_2, HO_2) play an important role as intermediates in the atmospheric oxidation and combustion of hydrocarbons. In polluted environments, alkylperoxy radicals (RO_2) and hydroperoxy (HO_2) react mostly with nitric oxide (NO).[1] Once peroxy radicals react with NO, a chain reaction yields tropospheric ozone (O_3), which causes respiratory problems for humans and animals.

Hydrocarbons undergo a hydrogen-atom abstraction, mostly by OH in the troposphere. The resulting alkyl radical (R) reacts almost exclusively with O_2 due to the rapid reaction rates and the abundance of O_2. The formation mechanism can be generalized by the following:

$$RH + (OH, NO_3, \text{or } Cl) \rightarrow R + (H_2O, HNO_3 \text{ or } HCl) \quad (1)$$

$$R + O_2 + M \rightarrow RO_2 + M \quad (2)$$

where M is any third body. In remote, clean areas of the troposphere, peroxy radicals terminate by reacting with HO_2 (reaction 3) and therefore no O_3 is formed.[1]

$$RO_2 + HO_2 \rightarrow ROOH + O_2 \quad (3)$$

One of the major sources of tropospheric HO_2 is formaldehyde photolysis. Carbon monoxide is a by-product in the mechanism, and the oxidation of CO by OH will yield yet another HO_2.

$$HCHO + h\nu \rightarrow H + HCO \quad (4)$$

$$H + O_2 + M \rightarrow HO_2 + M \quad (5)$$

$$HCO + O_2 \rightarrow HO_2 + CO \quad (6)$$

$$OH + CO \rightarrow CO_2 + H \quad (7)$$

$$H + O_2 + M \rightarrow HO_2 + M \quad (8)$$

In urban areas, reaction 3 competes with reaction 9 and its subsequent chain reaction shown below:

$$RO_2 + NO \rightarrow RHO + NO_2 \quad (9)$$

$$RHO + O_2 \rightarrow RO + HO_2 \quad (10)$$

$$HO_2 + NO \rightarrow HO + NO_2 \quad (11)$$

$$NO_2 + h\nu \rightarrow O + NO \quad (12)$$

$$O + O_2 + M \rightarrow O_3 + M \quad (13)$$

A single RO_2 can be responsible for the production of two O_3 molecules when reaction 9 is dominant over reaction 3. With an $[HO_2]$ of 1×10^8 molecules cm^{-3}, reaction 9 becomes competitive with reaction 3 when there is only half that amount of NO.[1]

1.1.2 Hydroperoxy Radical

HO_2 is the simplest peroxy radical and the one found in the largest concentrations in the atmosphere (peak concentrations between 10^8–10^9 molecules cm^{-3}). It is an important atmospheric component (see reactions 11–13). In the presence of water vapor, previously ignored in many studies, a significant enhancement of the self-reaction rate occurs.[2-4]

$$HO_2 + HO_2 \rightarrow HOOH + O_2 \quad (14)$$

$k_{14} = (2.2 \pm 0.3) \times 10^{-12}$ cm^3 $molecule^{-1}$ s^{-1} at 295 K Reference 5

$$HO_2 + HO_2 \cdot H_2O \rightarrow HOOH + O_2 + H_2O \quad (15)$$

$k_{15} = 3.3 \times 10^{-12}$ cm^3 $molecule^{-1}$ s^{-1} at 295 K Reference 6

The reaction mechanism includes a formation of an HO_2-H_2O complex which acts as an energy chaperone that removes excess energy from the activated complex on the potential energy surface so products can more easily be formed.

Modeling studies that involve this reaction rate include chemical cloud models, studies of marine environments, and three-dimensional global simulations. Satellites and air-borne balloons can be used to track HOOH, whose main source is the HO_2 self-reaction (see reactions 14 and 15). The photolysis of HOOH is a source of more HO_x radicals that deplete ozone levels in the stratosphere. With a known [HOOH], photolysis rate, and an accurate k_{14} and k_{15}, the concentration of HO_2 can be determined from modeling. For accurate modeling, we need to know the effect of water vapor on k_{15}. If only k_{14} is used in atmospheric modeling studies, predictions underestimate hydrogen peroxide (HOOH) formation and overestimate HO_2, O_3, and other organic peroxide concentrations according to Stockwell.[6] He reports that these models show discrepancies from empirical data because they have ignored the water dependence of either one or both of the bimolecular and the pressure dependent terms in the overall rate constant. The water vapor enhancement is observed to increase with decreasing temperatures, which could be due to the lowered kinetic energy in the HO_2-H_2O complex. Stockwell calculated the HO_2 self-reaction rate coefficient as a function of altitude, assuming a water vapor-saturated standard atmosphere. His work showed that omission of the water dependence on the overall rate coefficient would result in a 75 % relative error when modeling HOOH formation rates under atmospheric conditions typical of the lower troposphere. Stockwell concluded that the water vapor concentration term in the HO_2 self-reaction rate coefficient could not be ignored when modeling tropospheric chemistry.

Recently, the existence of the HO_2-H_2O complex has been confirmed by Suma et al. [8], who measured the microwave spectrum of the complex in a supersonic jet by means of a Fourier transform microwave spectrometer. The binding energy of the complex (6.9 kcal mol^{-1}) was predicted by Aloisio and Francisco[9] using *ab initio* molecular methods. Kanno et al. [4], using frequency modulated diode laser spectroscopy, have successfully measured the equilibrium constant of the HO_2-H_2O complex at 298K. These measurements, combined with measured water vapor concentration, suggest that 20–30 % of the HO_2 radicals may exist as the complex under typical atmospheric conditions.

1.1.3 Methylperoxy Radical

Because water is ubiquitous in the atmosphere with concentrations [6] ~10^{17} molecules cm^{-3}, we speculated that water could be complexing with other RO_2 radicals in much the same way it complexes with HO_2 radical. The efforts of this study have been focused on the role of organic RO_2-H_2O complexes, in particular CH_3O_2.

Methyl peroxy is formed during the photooxidation of methane (CH_4) shown in reactions 1 and 2. CH_4 is a naturally occurring component of the troposphere[1] (~1.7 ppm or 4.18×10^{13} molecules cm^{-3}). The main sources are anaerobic bacterial fermentation in wetlands and enteric fermentation mostly from cattle. Humans may be indirectly responsible for the increase in tropospheric CH_4 over the past three decades (increasing 1–2 % annually).[1] As the human population increases, so does the need for food; to produce more rice and beef requires more rice fields and livestock, which are both sources of CH_4.

One of the threats that CH_4 poses to humans is not in remote areas, but in polluted areas specifically with significant levels of NO concentrations. Instead of reaction 3, the following occurs for CH_3O_2:

$$CH_3O_2 + NO \rightarrow CH_3O + NO_2 \quad (16)$$

$$CH_3O + O_2 \rightarrow HCHO + HO_2 \quad (17)$$

$$HO_2 + NO \rightarrow HO + NO_2 \quad (18)$$

$$NO_2 + h\nu \rightarrow O + NO \quad (19)$$

$$O + O_2 + M \rightarrow O_3 + M \quad (20)$$

The amount of O_3 increases with CH_3O_2 with increasing sources of CH_4.

The self-reaction of CH_3O_2 is currently considered too slow to be a significant loss process under atmospheric chemistry, except in pristine environments where there is minimal NO concentrations.

$$CH_3O_2 + CH_3O_2 \rightarrow \text{Products} \quad (21)$$

$$k_{21} = 1 \times 10^{-13} \exp(365/T) \text{ cm}^3 \text{ molecule}^{-1} \text{ s}^{-1} \quad \text{Reference 10}$$

$$CH_3O_2 + CH_3O_2 \cdot H_2O \rightarrow \text{Products} \quad (22)$$

If a rate enhancement were observed in the presence of water vapor, then the new rate constant could have a significant effect on modeling behavior.

In a recent high level *ab initio* study, Clark et al. [11] reported on the optimized geometries, binding energies, and equilibrium constants for a series of organic peroxy radical-water complexes. Their work showed that for species with strong binding energies (~ 5-7 kcal mol^{-1}) a significant fraction (10 - 25 %) of the RO_2 radicals can exist as an RO_2-H_2O complex. They reported that the binding energy of the complexes is largest when the R-group in the peroxy radical includes a carbonyl (C=O) or alcohol (-OH) moiety. We have investigated the influence of water vapor on the kinetics of both the CH_3O_2 self-reaction and the $CH_3O_2 + HO_2$ reaction. As a consequence of the weak binding energy between the methyl peroxy radical and water (3.2 kcal mol^{-1}), the equilibrium constant for formation of a CH_3O_2-H_2O complex is very small (1.54

$\times 10^{-21}$ cm^3 $molecule^{-1}$, at 298 K). As a result, a methyl peroxy-water complex is not expected to form and consequently will not participate during the reaction mechanism of the CH_3O_2 self-reaction. The possible enhancement in the $CH_3O_2 + HO_2$ reaction kinetics was hypothesized because of the formation of an HO_2-H_2O complex during the reaction mechanism.

$$CH_3O_2 + HO_2 \rightarrow CH_3OOH + O_2 \quad (23)$$

$$k_{23} = 3.8 \times 10^{-13} e^{(800/T)} \text{ cm}^3 \text{ molecule}^{-1} \text{ s}^{-1} \quad \text{Reference 12}$$

$$CH_3O_2 + HO_2 \cdot H_2O \rightarrow CH_3OOH + O_2 \quad (24)$$

A rate enhancement would increase the competition between reactions 24 and 16.

1.2 Experimental Techniques

Laser flash photolysis/UV time-resolved spectroscopy was used to generate and detect the peroxy radicals. Molecules were photolyzed by a 351 nm excimer laser flash of ~300 mJ pulsing at 2 Hz. The radicals formed following photolysis initiate more reactions that lead to the molecules of interest. To be detectable by the system, the molecules must absorb UV light. Peroxy radicals characteristically absorb between 200 and 300 nm. The absorbances of HO_2 and CH_3O_2 have been previously characterized, but they do overlap (see Figure 1). So, multiple species can absorb around the wavelengths of the molecule of interest. We overcame this by only measuring HO_2 in excess at 220 nm and by measuring CH_3O_2 at 260 nm where HO_2 minimally absorbs.

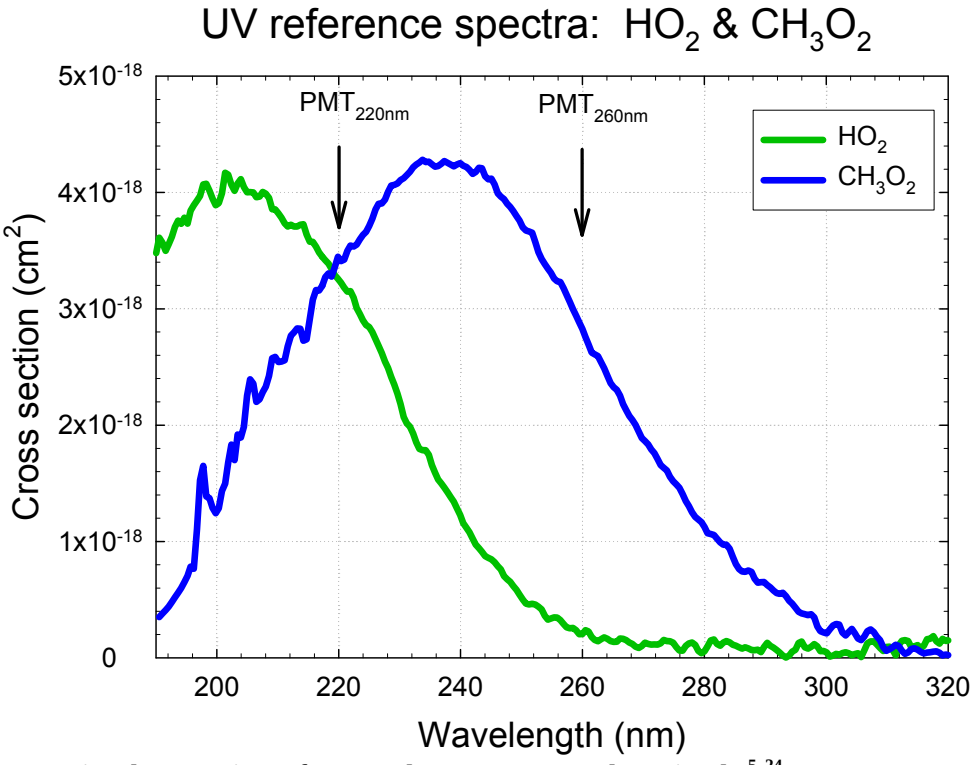

Figure 1 Cross sectional comparison of HO_2 and CH_3O_2 measured previously.[5, 24]

Because water has many absorbance lines in the infrared, locating and resolving a line is done by use of a tunable diode laser (TDL). This study uses a cryogenically cooled (77 K) Pb-salt TDL that is tuned to an absorption line at 1524 cm^{-1}.corresponding to the H-O-H bend in H2O.

CHAPTER 2: EXPERIMENTAL

To investigate the water vapor dependence on the rate of reaction involving RO_2 radicals, the kinetics of the self-reactions of HO_2 and CH_3O_2 as well as the cross-reaction of HO_2 + CH_3O_2 were measured over 263-303 K at ~200 Torr. Flash photolysis/UV spectroscopy is used to evaluate the kinetics and radical concentrations while tunable diode laser (TDL) spectroscopy is used to quantify the water vapor concentration. While it is expected that the rate enhancement is temperature dependent, the range of temperatures is limited due to the decrease in water vapor pressure at temperatures below 273 K and the expected drop in the rate enhancement at temperatures above 295 K.

All of the experiments are performed in a quartz cylindrical reaction cell (52.8 cm in length, 3.6 cm in diameter) which is wrapped in an insulated jacket connected to a recirculating cooler. K-type thermocouples are placed at the ends of the cell to monitor the temperature of the system. BaF_2 windows are used at both ends of the cell because they transmit both UV and IR light over the range of interest. Dichroic mirrors are coated to reflect 351 nm light with a bandpass of 10 nm around the center wavelength, direct the excimer laser beam and allow counter-propagation of the Xe lamp beam (Oriel 60010).

2.1 Peroxy Kinetics Measurements

CH_3O_2 and HO_2 are formed in the reaction cell using a gas mixture containing 4-6 Torr of 5 % Cl_2/N_2, 0.2-1 Torr of CH_3OH (99.93 % ACS HPLC grade) carried by N_2 or 75−100 Torr of CH_4, 20 Torr of O_2 and enough N_2 to reach a total pressure of 175 to 250 Torr. Tylan mass flow controllers adjust the gas flows (of Cl_2, CH_4, O_2, N_2) to achieve the appropriate partial pressures. The flow rates are verified by measuring the rate of pressure change measured by MKS pressure gauges when a selected gas flows into a fixed volume flask. CH_3OH is introduced with a syringe

pump (kd Scientific model 100) at a rate of 2.0-2.4 mL/hr using N_2 as the carrier gas. The CH_3OH is injected into a heated line (~373 K) of N_2 where it evaporates and mixes before being introduced into the reaction cell. The vapor concentration of CH_3OH is calculated from the molar concentration using the syringe delivery rate and the flow of the carrier gas in standard liters per minute along with the temperature of the cell, the density of methanol and other system factors. $[CH_3OH]$ is adjusted by changing the syringe delivery rate and/or the carrier gas flow rate. For the CH_3O_2+HO_2 reaction, both methane and methanol are flowed and the ratio of $[CH_4]/[CH_3OH]$ determines the relative concentrations of CH_3O_2 and HO_2. This ratio was between 90 and 120.

The chemistry is initiated with an excimer laser (Lamda Physik model Compex 205) using a XeF mixture which produces 351 nm light and is operated at 2 Hz and 280-320 mJ $pulse^{-1}$. The laser photolyzes a small fraction (1 - 3 %) of the Cl_2 to produce Cl radicals. The initial concentration of Cl is in the range of $(3\text{-}7) \times 10^{14}$ $molecules/cm^3$. It is measured by substituting ethane as the reactant to generate ethyl peroxy radicals. For the conditions used in these experiments, 98% of the Cl radicals are converted to ethyl peroxy radicals via the following mechanism:

$$Cl_2 + h\nu(351\ nm) \rightarrow 2Cl\cdot \quad (25)$$

$$Cl\cdot + C_2H_6 \rightarrow C_2H_5 + HCl \quad (26)$$

$$C_2H_5 + O_2 \rightarrow C_2H_5O_2 \quad (27)$$

Similarly, the chlorine atoms abstract H atoms from either CH_4 or CH_3OH, depending on the reaction to be studied, to ultimately produce CH_3O_2 or HO_2 radicals, respectively. The mechanism for HO_2 formation is:

$$Cl\cdot + CH_3OH \rightarrow CH_2OH + HCl \quad (28)$$

$$CH_2OH + O_2 \rightarrow HO_2 + CH_2O \quad (29)$$

$$HO_2 + HO_2 \rightarrow HOOH + O_2 \quad (14)$$

$$HO_2 + HO_2{\cdot}H_2O \rightarrow HOOH + O_2 + H2O \quad (15)$$

The same Cl radical chemistry initiates the production of CH_3O_2 via

$$Cl{\cdot} + CH_4 \rightarrow CH_3 + HCl \quad (29)$$

$$CH_3 + O_2 \rightarrow CH_3O_2 \quad (30)$$

$$CH_3O_2 + CH_3O_2 \rightarrow \text{Products} \quad (21)$$

$$CH_3O_2 + CH_3O_2{\cdot}H_2O \rightarrow \text{Products} \quad (22)$$

The cross-reaction is also measured in the presence and absence of water vapor using the same initiation processes shown above followed by:

$$CH_3O_2 + HO_2 \rightarrow CH_3OOH + O_2 \quad (23)$$

$$CH_3O_2 + HO_2{\cdot}H_2O \rightarrow CH_3OOH + O_2 \quad (24)$$

The reactions included in Table 1 include those already provided as well as secondary reactions involving reactants and/or intermediate products. The reactions listed in Table 1 sufficiently describe the chemistry in the cell for the following reasons: (1) the gas mixture is continuously replenished every 2 seconds, the products are removed from the reaction cell and the reactant concentrations are restored between photolysis events, (2) Due to its small cross-section, < 3% of the Cl_2 is photolyzed, and therefore the mixing of the cell eliminates secondary reactions, (3) The excimer beam is only photolyzing a small area (1 cm^2) of the 3.6 cm diameter cell so each pulse of the laser is essentially photolyzing a fresh reaction cell, (4) The RO_2 chemistry is over in less than 5 ms, so the firing of the laser every 500 ms does not cause distortions in the chemistry of interest.

Table 1 Reactions used to predict peroxy radical reaction rate constants in the kinetic model.

# in text	Reaction	k (cm^3 $molecule^{-1}s^{-1}$)	reference
28	$CH_3OH + Cl \rightarrow CH_2OH + HCl$	5.50×10^{-11}	14
29	$O_2 + CH_2OH \rightarrow HO_2 + CH_2O$	9.60×10^{-12}	14
14	$HO_2 + HO_2 \rightarrow HOOH$	$2.81 \times 10^{-13}\ e^{(594/T)}$	5
29	$CH_4 + Cl \rightarrow CH_3 + HCl$	$6.6 \times 10^{-12}\ e^{(-1240/T)}$	14
30	$CH_3 + O_2 \rightarrow CH_3O_2$	$1.79 \times 10^{-12}\ (T/298)^{-1.70}$	12
21	$CH_3O_2 + CH_3O_2 \rightarrow 2CH_3O + O_2$	$1 \times 10^{-13}\ e^{(365/T)}$	10
23	$HO_2 + CH_3O_2 \rightarrow CH_3OOH + O_2$	$3.8 \times 10^{-13}\ e^{(800/T)}$	12
34	$CH_3 + Cl_2 \rightarrow CH_3Cl + Cl$	$4.78 \times 10^{-12}\ e^{(-240/T)}$	16
35	$CH_3 + Cl \rightarrow CH_2 + HCl$	2.56×10^{-10}	17
36	$CH_3 + CH_3 \rightarrow$ Products	6.00×10^{-11}	18
37a	$Cl + CH_3O_2 \rightarrow CH_3O + ClO$	7.3×10^{-11}	15
37b	$\rightarrow CH_2OO + HCl$	7.6×10^{-11}	15
38	$ClO + CH_3 \rightarrow$ Products	1.3×10^{-10}	22
39	$ClO + HO_2 \rightarrow HO_2 + HOCl$	6.2×10^{-12}	21
40	$ClO + CH_3O_2 \rightarrow CH_3O + ClOO$	4.9 × 10-12 $e^{(-330/T)}$	10
41	$ClO + ClO \rightarrow$ Products	1×10^{-14}	14
42	$CH_3O + O_2 \rightarrow CH_2O + HO_2$	$7.2 \times 10^{-14}\ e^{(1080/T)}$	14
43	$CH_3O + CH_3O \rightarrow CH_2O + CH_3OH$	3.85×10^{-11}	19
44	$CH_3O_2 + CH_3O \rightarrow$ Products	2.62×10^{-12}	20

It is important to note that the reaction between water vapor and chlorine is an insignificant (<< 1 %) loss process for either chlorine atoms or water vapor owing to the extremely small rate constant for this reaction (k_{300K}=2.03 × 10^{-23} cm^3 $molecule^{-1}$ s^{-1}).[13] Fluorine

would have served as a more efficient initiator, however the F radical reacts very quickly with water and would result in secondary reactions.

Figure 2 shows the main components and layout of the experimental apparatus. Time-resolved detection of HO_2 and CH_3O_2 radicals is made by directing the output from an Xe arc lamp (Oriel 60010) through the reaction cell. The laser photolysis beam path is aligned to pass coaxially with the UV probe path by the use of dielectric mirrors which reflect the 351 nm photolysis beam while passing all other UV wavelengths (with the exclusion of a ± 15 nm band centered around 351 nm). UV light absorption is detected by a monochromator (Instruments SA, Inc. model HR 320, grating 147 line/mm) and photomultiplier tube (EMI 9558QB). The signal is amplified and sent to a digital oscilloscope. The concentration of CH_3O_2 radicals is measured by monitoring the signal at 260 nm, and HO_2 is monitored at 220 nm. These wavelengths are used to distinguish between the two radicals based on their cross-sections shown previously in Figure 1. HO_2 absorbs very weakly at 260 nm and so does not interfere significantly with CH_3O_2 detection. Their cross sections are nearly equal at 220 nm which is why we only monitor HO_2 self–reaction as 220 nm.

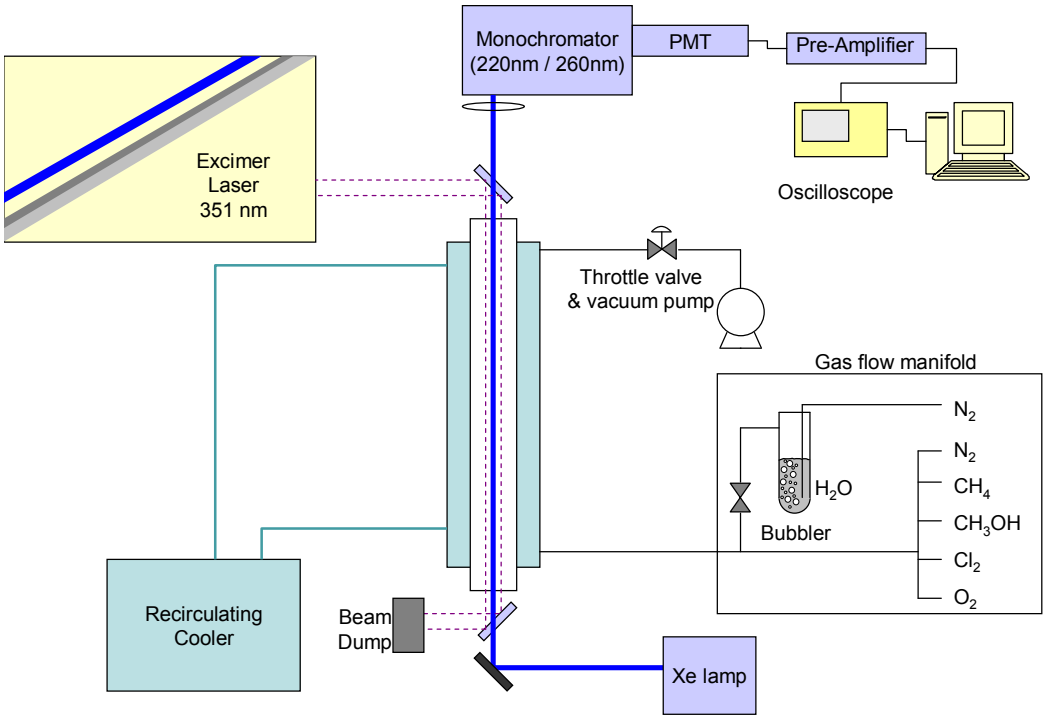

Figure 2 Schematic of UV system for kinetic measurements

The measurement of the absorbance below 220 nm was considered unsuitable because the quality of the signal fell off sharply due to the response of the PMT and the Xe lamp output. Typically, 400 individual decays from the PMT are co-added and averaged to produce a decay with sufficient S/N. The oscilloscope (Tektronix Model 460A, sampling rate 2 μs/pt and 12 bit resolution) is triggered by a photodetector activated by the laser flash. Transient behavior is recorded for 0.5 ms before photolysis and 4.5 ms after photolysis using a data acquisition rate of 2 μs. This provides appropriate time resolution to monitor the transient behavior of the peroxy radical reactions over a sufficient duration for the chemistry to proceed.

2.2 Water Concentration Measurements

2.2.1 Bubbler

Water vapor is introduced into the reaction cell by N_2 carrier gas passing through a bubbler immersed in a constant temperature bath. The amount of water is controlled by both the temperature of the water and the flow rate of the carrier gas. Three concentrations of water are produced by adjusting the temperature of the water or by adjusting the flow rate of carrier gas.

2.2.2 IR detection of water vapor

TDL IR spectroscopy is used to quantify the water in the cell. Figure 3 shows a schematic of the IR system illustrating the use of separate lock-in amplifiers and detectors for the reaction cell and the reference cell. The water absorbs IR light that is scanned over a narrow frequency band centered at the 1524 cm^{-1} line such that the entire peak of the selected rovibration transition can be observed. The IR beam is produced by a Pb-salt TDL (Laser Components, Serial #9124263) that is tuned by a current and temperature controller (model L5830) and mounted in an LN_2 dewar (model L5736). The beam passes through a monochromator that determines its IR frequency, ± 1cm^{-1}. It passes through a beam splitter where a portion of the beam is directed

through a reference cell containing a sample of water vapor (~ 2 Torr, 10 cm length). The remainder of the beam is directed to the reaction cell. After the signal propagates through the reaction cell, a second monochromator (Instruments SA, Inc. model HR 640, 75 line/mm, 10 μm blaze grating) filters the beam which is then directed to an LN_2 cooled HgCdTe detector. The AC coupled detector responds to changes in light intensity and requires additional signal modifications to obtain absolute light intensity measurements. A mechanical chopper, operating at 400 Hz, is placed in the beam path. The resulting AC signal from the IR detector is converted to a low noise, highly stable DC output by a lock-in amplifier (Stanford Research Systems model SR850) that receives a reference signal from the chopper. A function generator (Wavetek model 29) externally ramps the output of the diode laser with a frequency of 0.1 Hz with 500 $mV_{peak\ to\ peak}$. This results in the IR frequency of the diode laser scanning across the water line of interest, covering a range of 0.2 cm^{-1}. The beam from the reference cell is focused onto a second HgCdTe detector and its signal is sent to a second lock-in amplifier (Spectra-Physics Model SP5020) which converts the AC signal to a DC output. The output signals for both detectors are recorded synchronously by a digital oscilloscope (Tektronix TDS 460A).

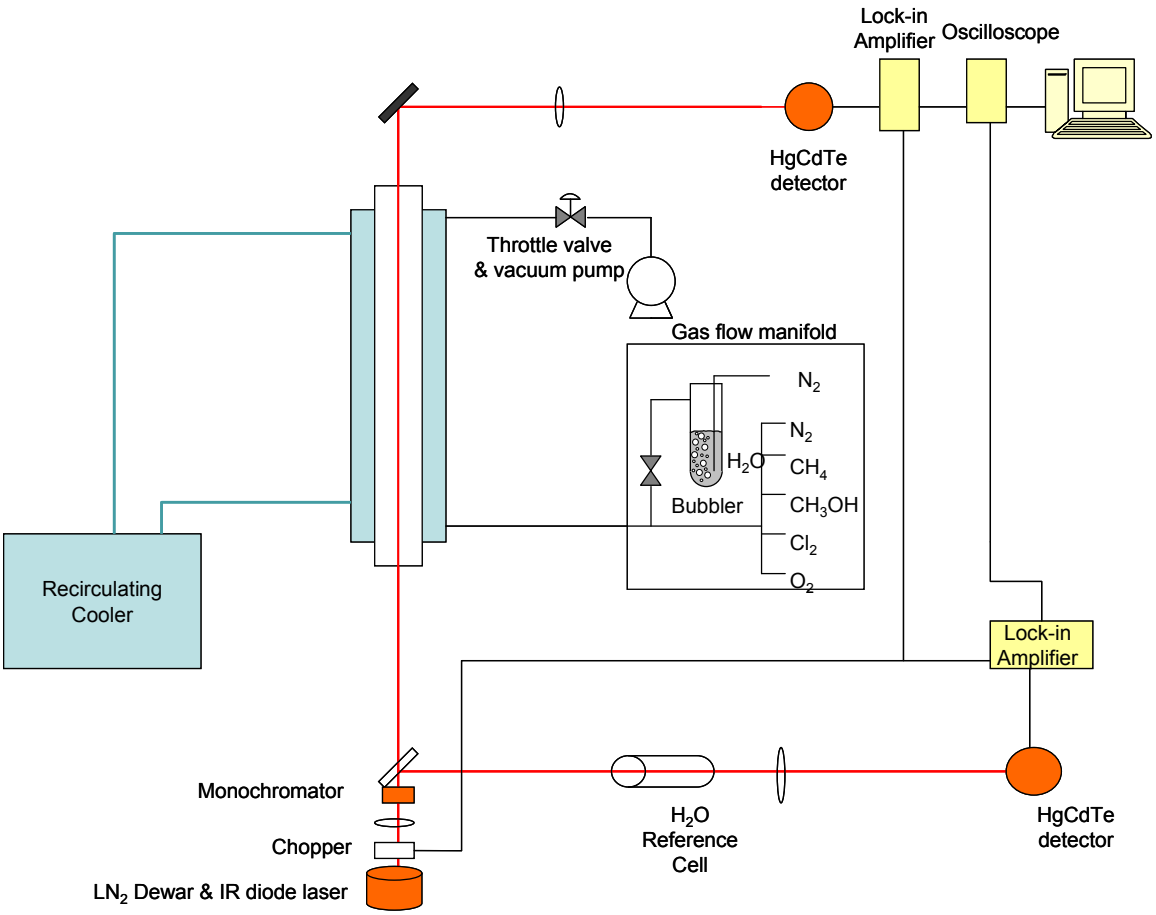

Figure 3 Schematic of IR system

2.2.3 Determination of the cross section of water

A syringe pump delivery system was used to introduce a known amount of water into the reaction cell over total pressures ranging from 50 to 700 Torr. Similar to quantifying methanol, the vapor concentration of water is calculated from the molar concentration using the syringe delivery rate, and the density and molecular weight of water. The flow rate of the carrier gas in standard liters per minute and the temperature and pressure of the mixture in the cell are needed to determine the [H_2O] for the range of conditions covered in this study. [H_2O] is adjusted by changing the syringe delivery rate and/or the carrier gas flow rate. The absorbance is calculated using the signal intensities from the IR scans of a dry cell (I_0) to a wet cell (I) and by using of Beer's Law. The cross section of water can then be then calculated.

$$\ln\left(\frac{Io}{I}\right) = A \tag{31}$$

$$\sigma = \frac{A}{\ell c} \tag{32}$$

where A is absorption, σ is the cross-section of the absorbing species, ℓ is the path length, and c is the concentration of the absorber. The signal intensities (I and I_0) were scanned across the absorbance line and the peak cross-section was calculated to be $2.0 \pm 0.2 \times 10^{-20}$ cm^2 at 200 Torr. The pressure dependent cross-section using the syringe pump system is shown in Figure 4. Figure 5 shows two measured spectra of water by the bubbler system at 273 and 295 K and indicates that there is no temperature dependence of the cross-section for the range of temperatures examined in this study. Since more water could be introduced with a bubbler (1 - 13×10^{16} cm^{-3}), the bubbler was used to generate water vapor instead of the syringe pump for the peroxy radical kinetics experiments. However, the water vapor concentration in the reaction flow cell produced by the bubbler was quantified using the same measurement technique with the IR absorbance measurement at 1524 cm^{-1} and applying the measured cross section.

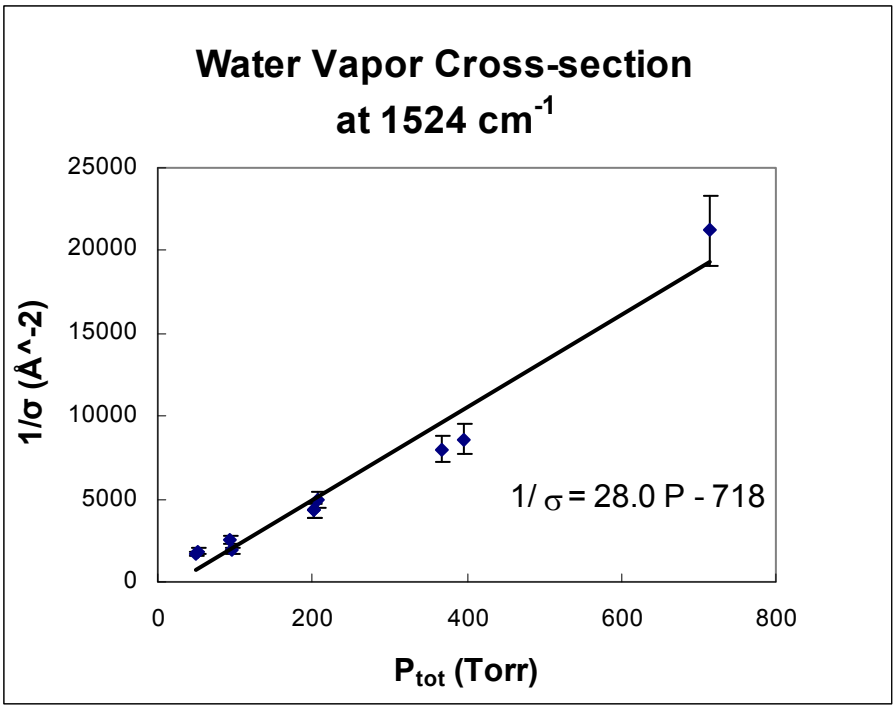

Figure 4 Pressure dependent cross-section of water vapor at 1524 cm^{-1}. [H_2O] is controlled by a syringe pump. Error bars show 10% error in the measured values. Line shown is a linear regression fit.

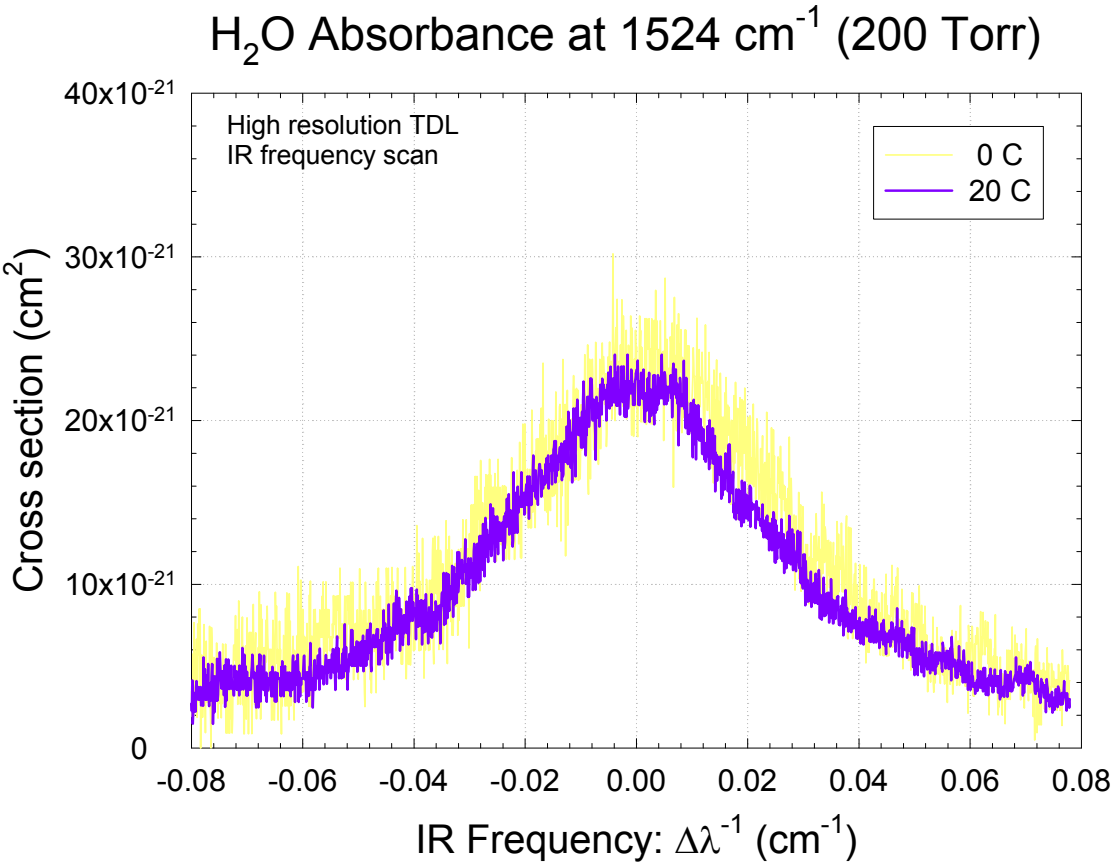

Figure 5 Water Absorbance of 1524 cm^{-1} light. Water vapor introduced by bubbler at 200 Torr and 273 K (yellow) or 295 K (blue).

CHAPTER 3: RESULTS

3.1 HO_2 + HO_2

The instrument and data collection technique was verified by measuring the HO_2 self-reaction as a function of water vapor and temperature. This reaction is an ideal candidate for calibration because the water vapor and temperature dependence have been previously reported.[2-4] Figure 6 shows typical HO_2 radical concentration/time decays in the presence and absence of water.

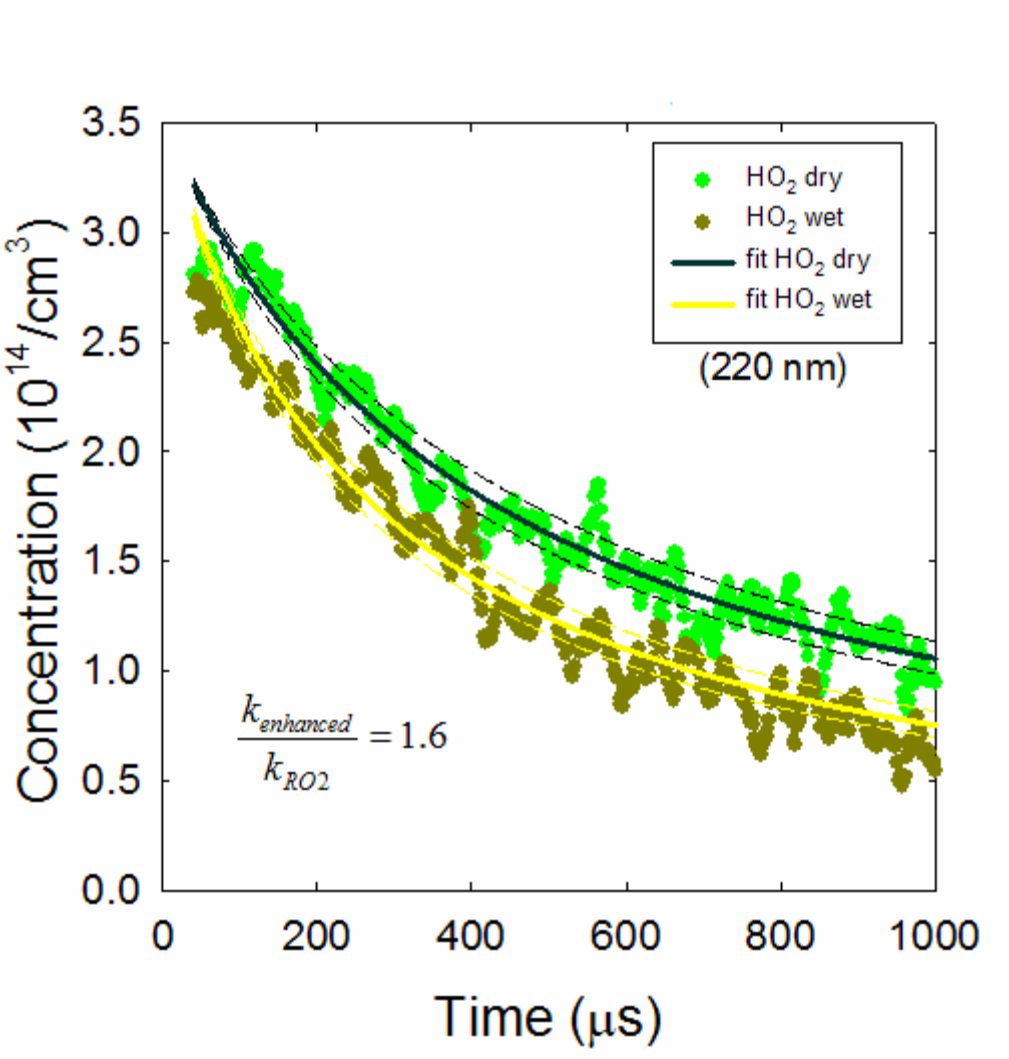

Figure 6 HO_2 self-reaction decays. Conditions: 175 Torr, 295 K, 5.3 Torr H_2O, Dashed lines show 10% uncertainty in the rate constant (uncertainty combined from calculated rate constants and from instrumental error).

The time/voltage traces collected by the PMT are converted to time/absorbance traces using equation 31, where I_0 is the averaged pre-trigger signal of each trace. Following this correction, equation 32 is used to calculate [HO_2] over the time range of interest. This time/concentration information is fit to a computational model that simultaneously solves a series of differential equations that describe the chemistry (Micromath Scientist version 2.01). For the HO_2 self-reaction the significant reactions are:

$$Cl\cdot + CH_3OH \rightarrow CH_2OH + HCl \quad (28)$$

$$CH_2OH + O_2 \rightarrow HO_2 + CH_2O \quad (29)$$

$$HO_2 + HO_2 \rightarrow HOOH + O_2 \quad (14)$$

$$HO_2 + HO_2\cdot H_2O \rightarrow HOOH + O_2 + H_2O \quad (15)$$

With the corresponding partial pressures of the reactants and the total pressure and temperature of the reaction cell, the model solves for the rate constant of the HO_2 self-reaction. At 295 K and no water, the rate constant was $(3.3\pm0.6) \times 10^{-12}$ cm^3 $molecule^{-1}$ s^{-1}, whereas at 295 K and 2.9×10^{17} molecules H_2O cm^{-3}, it was $(5.2\pm0.1) \times 10^{-12}$ cm^3 $molecule^{-1}$ s^{-1}. Maricq and Szente[15] reported the dry self-reaction rate as $(2.2\pm0.8) \times 10^{-12}$ cm^3 $molecule^{-1}$ s^{-1} at 295 K. This gives a rate enhancement of 1.6±0.1. At 285 K, the largest enhancement factor was observed, which is 1.8±0.1. These results compare favorably with Kircher and Sander who found an enhancement factor of ~1.8 at 285 K, 100 Torr, and a similar amount of water vapor.[2] A total of 28 experiments were carried out at temperatures between 263 K and 303 K. The maximum enhancement factor of 1.8±0.1 is seen at 283 K and 2.7×10^{17} molecules H_2O cm^{-3}. The enhancement was observed to be in the range of 0.9-1.8. Figure 7 shows the observed rate enhancement as a function of water vapor concentration for the various temperatures of the

reaction cell. Table 2 lists absolute rate constants determined in this study over the temperature and water vapor ranges.

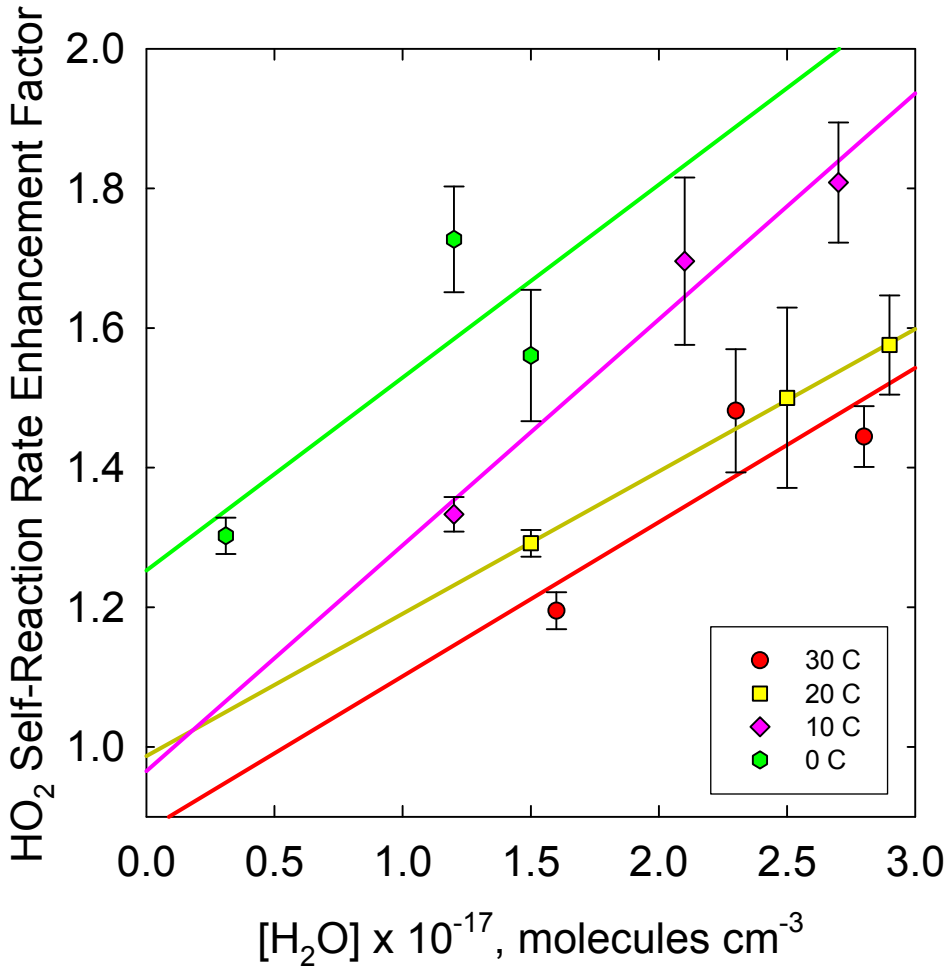

Figure 7 Enhancement (k_{wet}/k_{dry}) for HO_2 self-reaction rates performed at ~200 Torr and the specified temperature. Error was calculated from the uncertainties in the rate constants.

Table 2 Absolute rate constants for HO_2 self–reaction with and without water over the temperature and water vapor ranges. Total pressure was around 200 Torr. Overall uncertainty in the rate constants is 10% from the kinetics model and instrumental sources.

	HIGH WATER		MEDIUM WATER		LOW WATER	
TEMP (K)	$k_{wet} \times 10^{-12}$ (cm^3 $molecule^{-1}s^{-1}$)	$k_{dry} \times 10^{-12}$ (cm^3 $molecule^{-1}s^{-1}$)	$k_{wet} \times 10^{-12}$ (cm^3 $molecule^{-1}s^{-1}$)	$k_{dry} \times 10^{-12}$ (cm^3 $molecule^{-1}s^{-1}$)	$k_{wet} \times 10^{-12}$ (cm^3 $molecule^{-1}s^{-1}$)	$k_{dry} \times 10^{-12}$ (cm^3 $molecule^{-1}s^{-1}$)
303	2.7	3.9	2.7	4.0	2.4	2.9
295	3.3	5.2	2.4	3.6	2.4	3.1
283	4.7	8.5	2.3	3.9	2.7	3.6
273	6.6	10.3	2.8	4.9	4.3	5.6
263	12.4	13.8	6.9	6.2	7.8	9.2

3.2 $CH_3O_2 + CH_3O_2$

If the kinetics of the CH_3O_2 self-reaction showed water vapor dependence, it would likely be due to the formation of a CH_3O_2-H_2O complex during the reaction process, similar to the HO_2 self-reaction. Information about the probability of the formation of a CH_3O_2-H_2O complex including its binding energy, minimum energy structure and equilibrium constant was reported in the study by Clark, et al.[11] Due to the relatively weak binding energy of the CH_3O_2-H_2O complex (3.2 kcal mol^{-1}) and subsequent small equilibrium constant (1.54×10^{-21} cm^3 $molecule^{-1}$), it is unlikely that a sufficient concentration of the complex exists under atmospheric conditions. Using this K_{eq} and the water concentrations used in this study, the atmospheric abundance of the theoretical CH_3O_2-H_2O complex compared to the un-complexed CH_3O_2 complex can be calculated. Equation 33 gives the ratio.

$$K_{eq}[H_2O] = \frac{[RO_2 - H_2O]}{[RO_2]} \tag{33}$$

Using the three concentrations of H_2O at 295 K used in this study, the predicted fraction of the CH_3O_2-H_2O complex relative to the un-complexed is 0.02 - 0.05 %. The Kanno[4] equilibrium constant ($K_{eq} = (5.2 \pm 3.2) \times 10^{-19}$ cm^3 $molecule^{-1}$ at 293 K) predicts 7.8-15% HO_2-H_2O complexed under the conditions of our study.

Experimental determination for the lack of a water dependence on the CH_3O_2 self-reaction rate coefficient confirmed the theoretical work of Clark et al. The CH_3O_2 self-reaction rate coefficient in the presence of water vapor was measured using the same instrument/technique described previously. Figure 8 shows the time decays of CH_3O_2 in the absence and presence of water vapor at 295K.

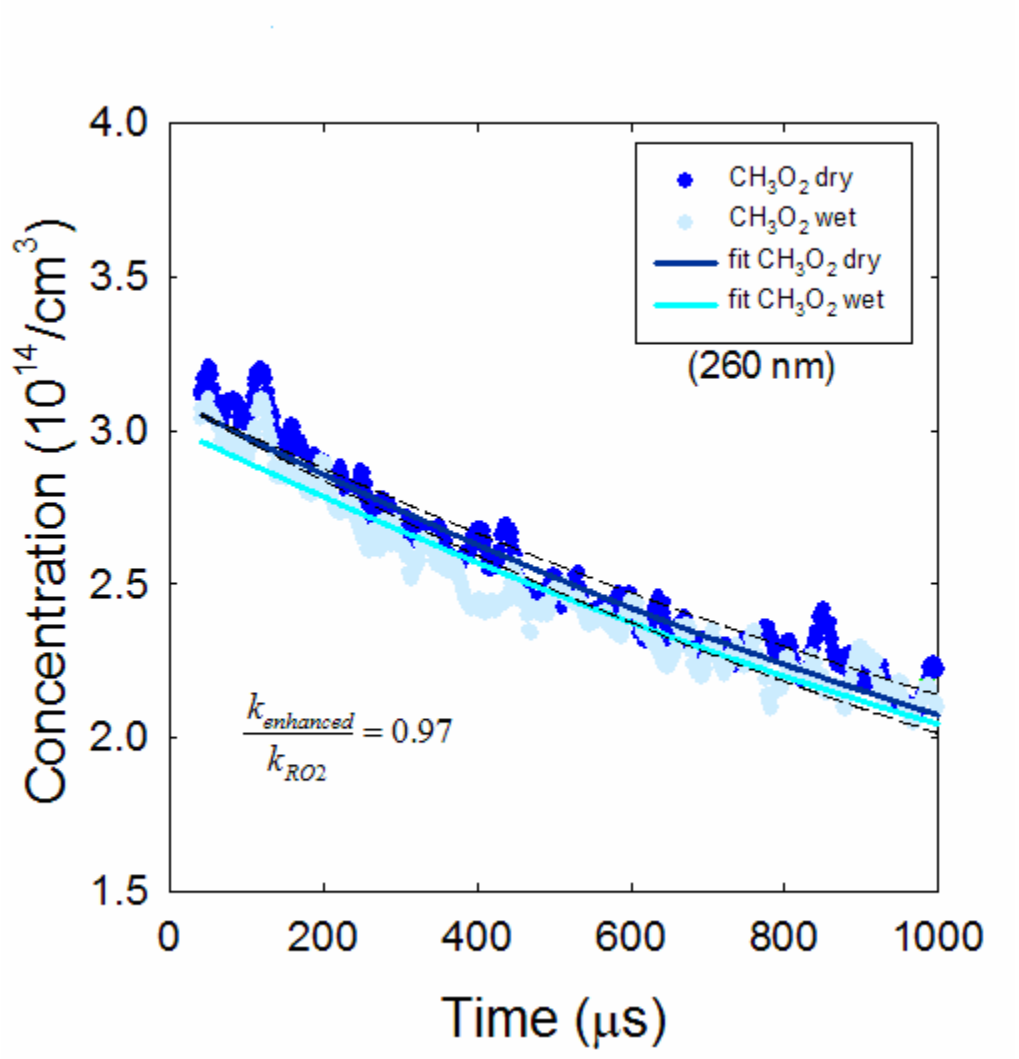

Figure 8 CH_3O_2 self-reaction decays. Conditions: 175 Torr, 295 K, 5.3 Torr H_2O, Dashed lines show 10% uncertainty in the rate constant (uncertainty combined from calculated rate constants and from instrumental error). About 0.05 % of the CH_3O_2 is complexed with H_2O.

The chemistry of CH_3O_2 is much more involved than HO_2. Below are the reactions used to model the decay of CH_3O_2:

Primary Reactions

$Cl\cdot + CH_4 \rightarrow CH_3 + HCl$ (29)

$CH_3 + O_2 \rightarrow CH_3O_2$ (30)

$CH_3O_2 + CH_3O_2 \rightarrow Products$ (21)

$CH_3O_2 + CH_3O_2\cdot H_2O \rightarrow Products$ (22)

Competing Reactions

$Cl_2 + CH_3 \rightarrow CH_3Cl + Cl$ (34)

$Cl\cdot + CH_3 \rightarrow CH_2 + HCl$ (35)

$CH_3 + CH_3 \rightarrow Products$ (36)

$Cl\cdot + CH_3O_2 \rightarrow CH_3O + ClO$ (37a)

$\rightarrow CH_2OO + HCl$ (37b)

$ClO + CH_3 \rightarrow Products$ (38)

$ClO + HO_2 \rightarrow HO_2 + HOCl$ (39)

$ClO + CH_3O_2 \rightarrow CH_3O + ClOO$ (40)

$ClO + ClO \rightarrow Products$ (41)

Secondary Reactions

$CH_3O + O_2 \rightarrow CH_2O + HO_2$ (42)

$CH_3O + CH_3O \rightarrow CH_2O + CH_3OH$ (43)

$HO_2 + HO_2 \rightarrow HOOH$ (14)

$HO_2 + CH_3O_2 \rightarrow CH_3OOH + O_2$ (23)

$CH_3O_2 + CH_3O \rightarrow Products$ (44)

Species in reactions 34–36 remove CH_3, but have little affect on the kinetics due to the abundance of O_2 in the reaction cell. Unlike the rapid formation of HO_2, CH_3O_2 forms slowly leaving enough Cl atoms to react with the peroxy radical and form ClO (reaction 37a). Approximately 3–4 % of Cl radicals are converted to ClO based on the rate of formation of CH_3O_2. Once formed, ClO has little effect on the decay of CH_3O_2 due to very slow reactions with other species (reactions 38–41). Consequently, the ClO has a long lifetime in the cell. With a cross-section ($\sim 5 \times 10^{-18}$ cm^2) nearly twice that of CH_3O_2 at 260nm, the ClO absorbance superimposes on the CH_3O_2 absorbance measured by the PMT. Because ClO absorbs across the entire region of the methyl peroxy spectrum, the detection wavelength cannot be shifted to avoid its contribution to the absorbance. Because of this interference, it is necessary to correct the measured absorbance for the ClO presence. The effect of the correction is less than 10 % on the absorbance used in the model. Oxidation of the methoxy radical (CH_3O) produces HO_2 which influences the kinetics of the CH_3O_2 peroxy radical (reaction 23).

At 295 K, k_{21} was $(5.7\pm0.2) \times 10^{-13}$ cm^3 $molecule^{-1}$ s^{-1} and at $[H_2O] = 2.9 \times 10^{17}$ molecules cm^{-3} k_{22} was $(5.3\pm0.2) \times 10^{-13}$ cm^3 $molecule^{-1}$ s^{-1}. Even with the maximum amount of water vapor, the observed decay appears to not be perturbed, as predicted by the K_{eq} calculated by Clark, et al. Atkinson et al. reported the self-reaction rate as 1.1×10^{-13} $e^{(365\pm201)/T}$ which is $(1.9 – 7.5) \times 10^{-13}$ cm^3 $molecule^{-1}$ s^{-1} at 295 K. A total of 21 experiments were carried out at temperatures between 263 K and 303 K. The maximum enhancement factor of 1.2±0.1 is seen at 263 K and 6.7×10^{16} molecules cm^{-3}, however, the enhancement typically was observed to be in the range of 0.9-1.2. Figure 9 shows the observed rate enhancement as a function of water vapor

concentration for the various temperatures of the reaction cell. Table 3 lists absolute rate constants determined in this study over the temperature and water vapor ranges.

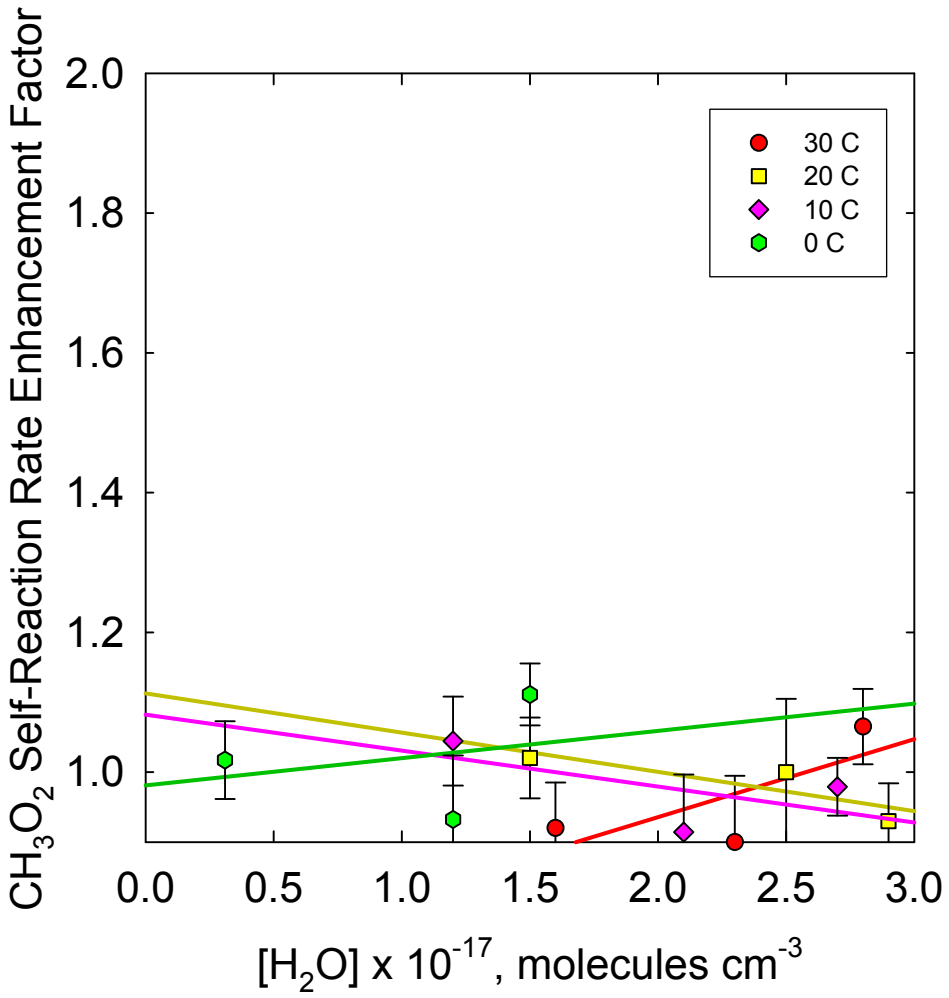

Figure 9 Enhancement (k_{wet}/k_{dry}) for CH_3O_2 self-reaction rates performed at ~200 Torr and the specified temperature. Error was calculated from the uncertainties in the rate constants.

Table 3 Absolute rate constants for CH_3O_2 self–reaction with and without water over the temperature and water vapor ranges. Total pressure was around 200 Torr. Overall uncertainty in the rate constants is 10% from the kinetics model and instrumental sources.

	HIGH WATER		MEDIUM WATER		LOW WATER	
TEMP (K)	$k_{wet}\times 10^{-13}$ (cm^3 $molecule^{-1}s^{-1}$)	$k_{dry}\times 10^{-13}$ (cm^3 $molecule^{-1}s^{-1}$)	$k_{wet}\times 10^{-13}$ (cm^3 $molecule^{-1}s^{-1}$)	$k_{dry}\times 10^{-13}$ (cm^3 $molecule^{-1}s^{-1}$)	$k_{wet}\times 10^{-13}$ (cm^3 $molecule^{-1}s^{-1}$)	$k_{dry}\times 10^{-13}$ (cm^3 $molecule^{-1}s^{-1}$)
303	4.6	4.9	3.0	2.7	5.0	4.6
295	5.7	5.3	5.9	5.9	4.9	5.0
283	4.8	4.7	3.5	3.2	4.5	4.7
273	9.9	11.0	5.9	5.5	5.8	5.9
263	8.2	9.4	4.6	4.7	4.6	5.5

3.3 CH_3O_2 + HO_2

Measurement of the $CH_3O_2 + HO_2$ reaction rate coefficient as a function of water vapor and temperature does not show any enhancement over the conditions probed. Figure 10 shows the decay of CH_3O_2 under conditions in which there is almost equal concentrations of HO_2 and CH_3O_2 in the reaction cell. The reaction has been run in the absence and presence of water vapor. For comparison purposes, the $[HO_2]$ was kept constant for these two runs. At 295 K, k_{23} was $(4.6- 9.5) \times 10^{-12}$ cm^3 $molecule^{-1}$ s^{-1} and k_{24} was $(4.7 - 9.6) \times 10^{-12}$ cm^3 $molecule^{-1}$ s^{-1} each with 5% uncertainty. Atkinson reported the self-reaction rate as $3.8 \times 10^{-13} e^{(800\pm400)/T}$ cm^3 s^{-1} which at 295 K falls between $1.5 - 22 \times 10^{-12}$ cm^3 $molecule^{-1}$ s^{-1}.

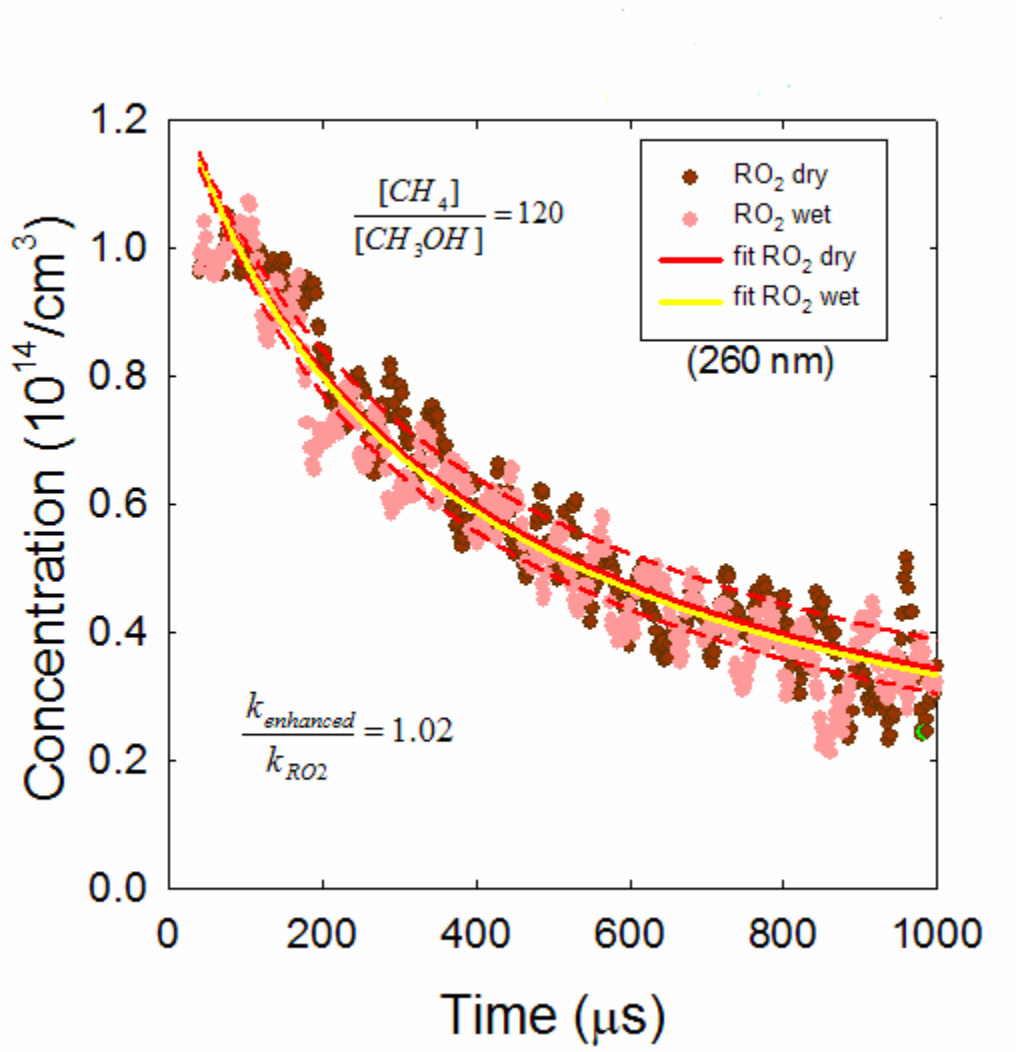

Figure 10 CH_3O_2 + HO_2 reaction decays. Conditions: 250 Torr, 295 K, 8 Torr H_2O, Dashed lines show 10% uncertainty in the rate constant (uncertainty combined from calculated rate constants and from instrumental error). About 7-15% of HO_2 is complexed with water.

With a significant [HO_2] in the cell, the chemistry becomes more competitive and complex. Below are the reactions used to model the decay of CH_3O_2 when HO_2 is present:

Primary Reactions

$$Cl\cdot + CH_3OH \rightarrow CH_2OH + HCl \quad (28)$$

$$CH_2OH + O_2 \rightarrow HO_2 + CH_2O \quad (29)$$

$$HO_2 + HO_2 \rightarrow HOOH + O_2 \quad (14)$$

$$HO_2 + HO_2\cdot H_2O \rightarrow HOOH + O_2 + H2O \quad (15)$$

$$Cl\cdot + CH_4 \rightarrow CH_3 + HCl \quad (29)$$

$$CH_3 + O_2 \rightarrow CH_3O_2 \quad (30)$$

$$CH_3O_2 + CH_3O_2 \rightarrow \text{Products} \quad (21)$$

$$HO_2 + CH_3O_2 \rightarrow CH_3OOH + O_2 \quad (23)$$

Competing Reactions

$$Cl_2 + CH_3 \rightarrow CH_3Cl + Cl \quad (34)$$

$$Cl\cdot + CH_3 \rightarrow CH_2 + HCl \quad (35)$$

$$CH_3 + CH_3 \rightarrow \text{Products} \quad (36)$$

$$Cl\cdot + CH_3O_2 \rightarrow CH_3O + ClO \quad (37a)$$

$$\rightarrow CH_2OO + HCl \quad (37b)$$

$$ClO + CH_3 \rightarrow \text{Products} \quad (38)$$

$$ClO + HO_2 \rightarrow HO_2 + HOCl \quad (39)$$

$$ClO + CH_3O_2 \rightarrow CH_3O + ClOO \quad (40)$$

$$ClO + ClO \rightarrow \text{Products} \quad (41)$$

Secondary Reactions

$$CH_3O + O_2 \rightarrow CH_2O + HO_2 \quad (42)$$

$$CH_3O + CH_3O \rightarrow CH_2O + CH_3OH \quad (43)$$

$$CH_3O_2 + CH_3O \rightarrow \text{Products} \quad (44)$$

Because of the CH_3OH presence in the cross-reaction, the [Cl] diminishes more quickly than it does in the CH_3O_2 self-reaction. Therefore, ClO cannot form in significant amounts due to

lack of available Cl radical, and it is unnecessary to correct the measured absorbance for the ClO presence taken at 260 nm.

A total of 26 experiments were carried out at temperatures between 263 and 303 K. The maximum enhancement factor of 1.2±0.1 is seen at 283 K and 2.7×10^{17} molecules H_2O cm^{-3}, however, the enhancement typically was observed to be in the range of 0.9-1.2. The enhancement factor is always calculated from reactions run consecutively and under the same conditions varying only the water presence or absence. Figure 11 shows the observed enhancement as a function of water vapor concentration for the various temperatures of the reaction cell. Table 4 lists absolute rate constants determined in this study over the temperature and water vapor ranges.

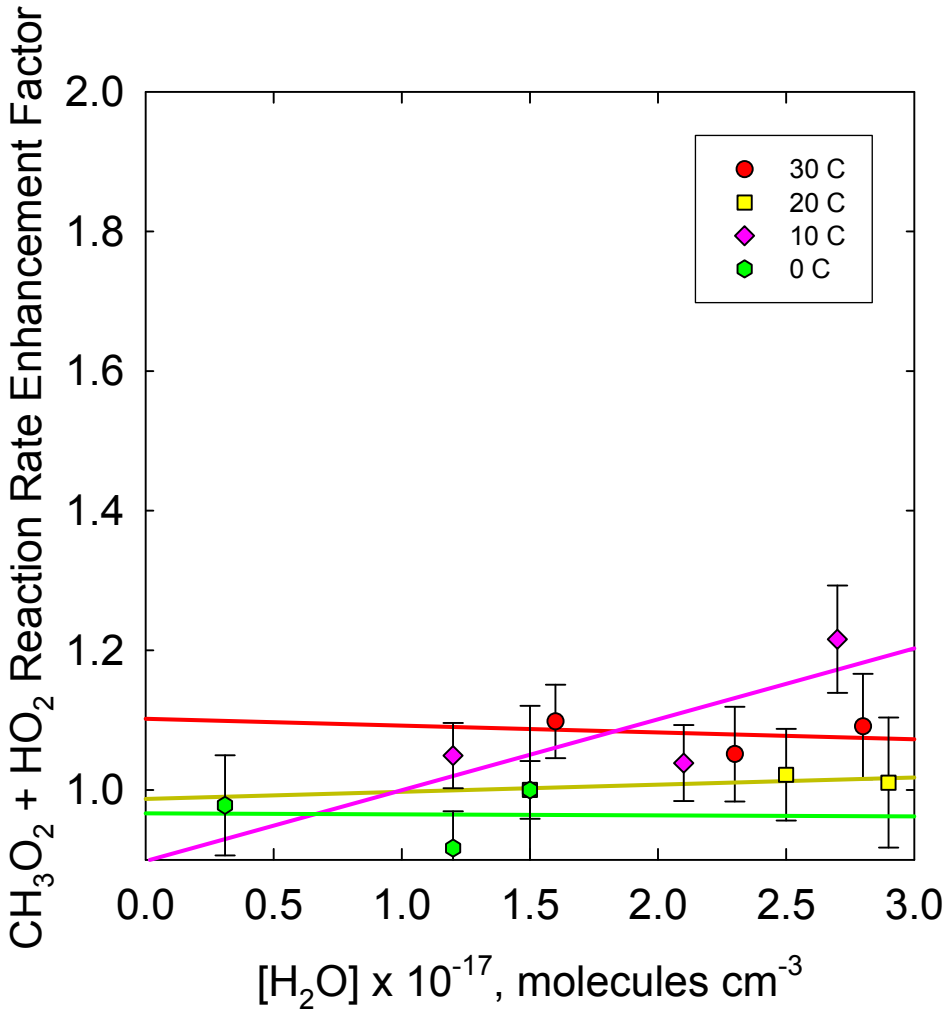

Figure 11 Enhancement (k_{wet}/k_{dry}) for $CH_3O_2 + HO_2$ reaction rates performed at ~200 Torr and the specified temperature. Error was calculated from the uncertainties in the rate constants.

Table 4 Absolute rate constants for CH_3O_2 + HO_2 reaction with and without water over the temperature and water vapor ranges. Total pressure was around 200 Torr. Overall uncertainty in the rate constants is 10% from the kinetics model and instrumental sources.

	HIGH WATER		MEDIUM WATER		LOW WATER	
TEMP (K)	$k_{wet}\times 10^{-12}$ (cm^3 $molecule^{-1}s^{-1}$)	$k_{dry}\times 10^{-12}$ (cm^3 $molecule^{-1}s^{-1}$)	$k_{wet}\times 10^{-12}$ (cm^3 $molecule^{-1}s^{-1}$)	$k_{dry}\times 10^{-12}$ (cm^3 $molecule^{-1}s^{-1}$)	$k_{wet}\times 10^{-12}$ (cm^3 $molecule^{-1}s^{-1}$)	$k_{dry}\times 10^{-12}$ (cm^3 $molecule^{-1}s^{-1}$)
303	8.8	9.6	3.9	4.1	5.1	5.6
295	9.5	9.6	4.6	4.7	5.8	5.8
283	8.8	10.7	5.2	5.4	6.1	6.4
273	9.8	9.8	4.8	4.4	9.1	8.9
263	10.5	10.3	6.7	7.0	5.9	6.4

3.4 Enhancement comparison for the three peroxy reactions of interest

Figures 12–14 show the rate enhancements of all three reactions at the various conditions of water vapor and temperature. The enhancement is consistently higher for the HO_2 self-reaction than the other reactions. None of the reactions showed enhancements at 263 K probably due the low concentration of water as a consequence of the saturation vapor pressure of water at that temperature.

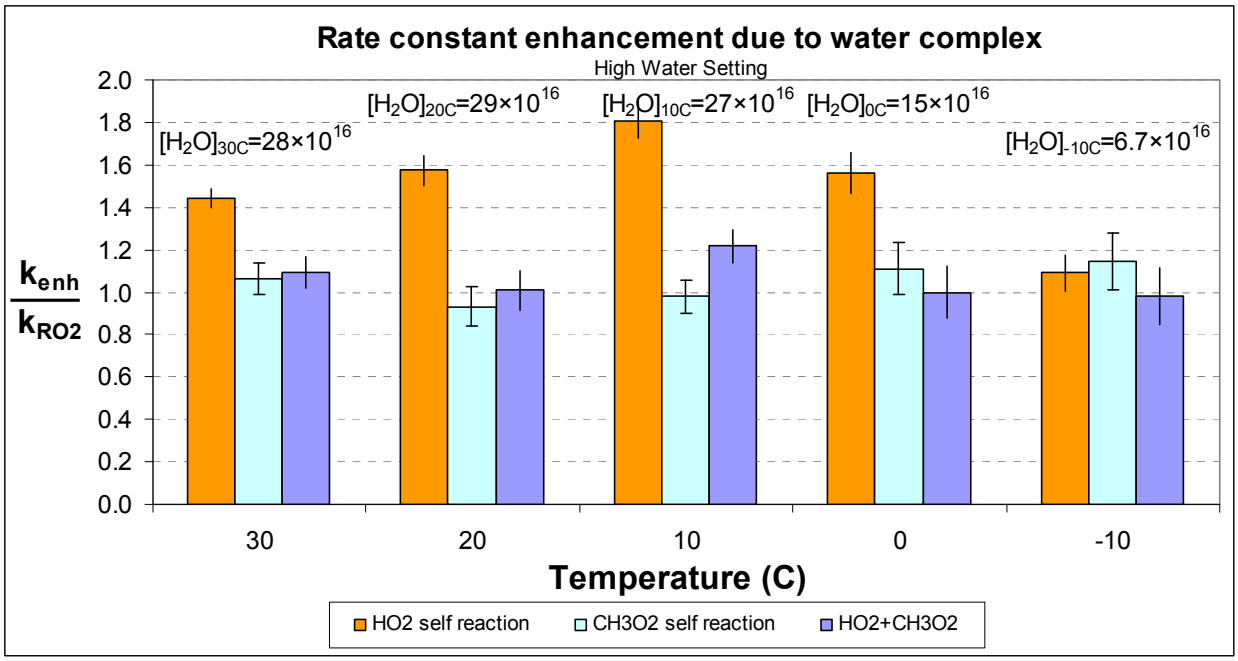

Figure 12 Comparison of reaction rate enhancement for the three reactions of interest at high concentration of water vapor. Reaction cell temperature is varied while the bubbler temperature and flow are constant. Bubbler at 25 C with ~3 SLPM N_2 flowing through.

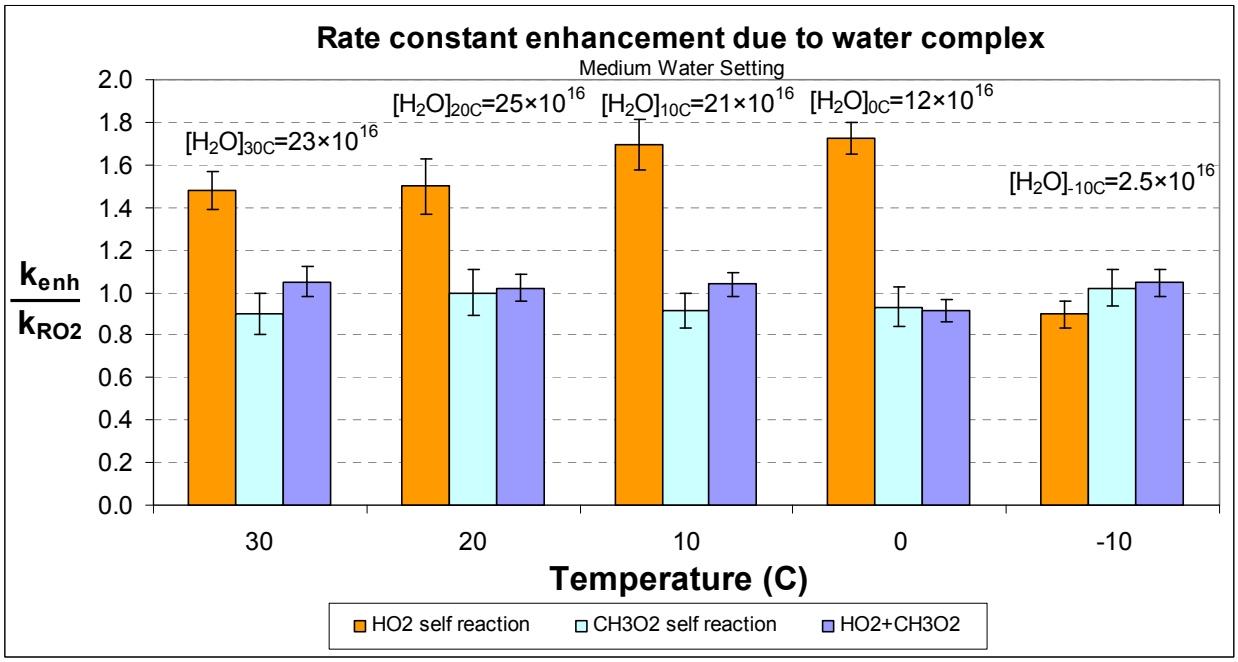

Figure 13 Comparison of reaction rate enhancement for the three reactions of interest at medium concentration of water vapor. Reaction cell temperature is varied while the bubbler temperature and flow are constant. Bubbler at 19 C with ~3 SLPM N_2 flowing through.

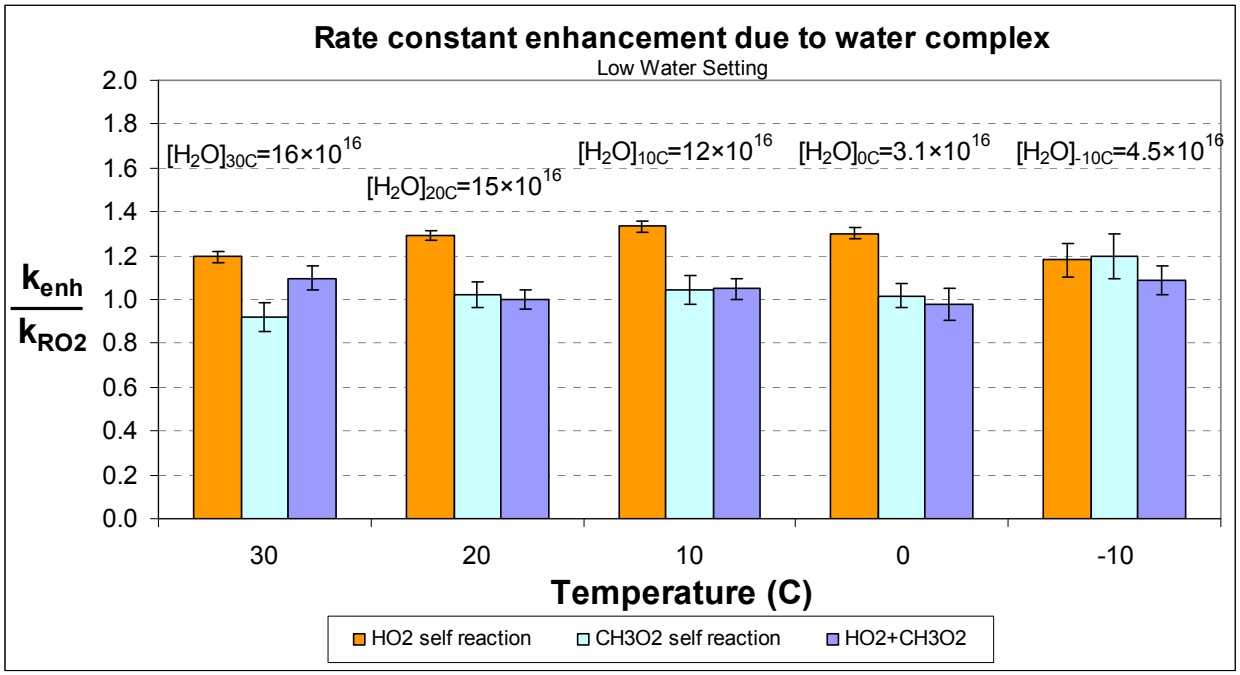

Figure 14 Comparison of reaction rate enhancement for the three reactions of interest at low concentration of water vapor. Reaction cell temperature is varied while the bubbler temperature and flow are constant. Bubbler at 19 C with ~1.5 SLPM N_2 flowing through.

3.5 Error Analysis

3.5.1 Experimental Measurements

Sources of uncertainty include the total pressure of the reaction cell from averaging the readings at the ends of the cell (±2%) and from the MKS pressure gauges which have an accuracy better than ±1%; K-type thermocouples measured the temperature at the ends of the cell and showed a gradient of 2%; uncertainty in the partial pressures of the gases is due to the measured flow rates (±2%) and the pressure gauges. Typically, 400 averages of the transient trace from the PMT was done to improve the S/N, but this also eliminates issues related to laser energy variation (<5%) which contributes to uncertainty in the $[Cl]_o$; Chopper accuracy of ±1mV (0.25%). This results in a 5% error in the rate constants from instrumental error.

Uncertainty in the measured cross section of water was 10% due to the accuracy of the syringe pump and the pressure gauges. When using the bubbler, the bath temperature could be controlled within 1 K. This results in a water vapor concentration uncertainty of ±10%.

3.5.2 Kinetics Model

The kinetics model uses a Jacobian Matrix to calculate the uncertainty in the calculated rate constants. Uncertainty is the 95% confidence level or two standard deviations from the value that was fitted from the individual absorbance decays collected. Referenced rate constant values were used in the model without any adjustments. The small uncertainties in the precursor gases did not affect the predictions of the model. A 5% uncertainty is attributed to the fit process of the rate constants giving an overall uncertainty of 10%. The uncertainty of the enhancement factor (k_{wet}/k_{dry}) shown is from the sum of the fractional uncertainties in the calculated rate constants.

CHAPTER 4: CONCLUSION

Clark et al. also calculated the potential energy surface (PES) of the $CH_3O_2 + HO_2$ and $CH_3O_2 + HO_2 \cdot H_2O$ on the triplet surface. To explain the rate enhancement seen for the HO_2-H_2O complex and the lack of rate enhancement for the other reactions, we examine the transition states from reactants to products. These radical-radical reactions occur when they are in close proximity so that they can form a closed shell species from their unpaired electrons. The transition state requires a collision from a third body to absorb the excess energy to prevent the activated complex from vibrating back to reactants. Once that excess energy is acquired by the third body (such as N_2), the activated complex reaches a minimum energy. Products will be more easily formed because of the reduction in transition state energy.

As mentioned previously, when water is part of the activated complex, it forms a complex with an HO_2 molecule. The enhancement of the self-reaction of HO_2 may be due to two factors. First, the water may be acting as an energy chaperone much like a third body except there is no delay for collisional frequency which must occur within the finite time before the transition state returns to reactants. In the case of the HO_2-H_2O complex, the "third body" is bound to the activated complex by 6.9 kcal mol^{-1}.[9] Second, the most efficient third body will mode match the activated complex which means it will have similar bonds that will more efficiently transfer energy. The OH stretch of HO_2 and H_2O couples easily because the frequencies (~3000 cm^{-1}) are similar.

Under the conditions probed, the CH_3O_2 self-reaction rate constant does not appear to be perturbed in the presence of water vapor. This is expected because of the inability of CH_3O_2 to form a complex with water as a consequence of the small binding energy. A larger binding energy indicates a larger K_{eq} which results in more RO_2-H_2O forming. Fewer CH_3O_2-H_2O

complexes form than HO_2-H_2O because of the smaller binding energy of CH_3O_2-H_2O (3.2 kcal mol^{-1}).[11] Not only are a smaller number of complexes formed, but there is inefficient coupling (mode matching) because of the dissimilar bonds and frequencies of those bonds in CH_3O_2 (C-H, C-O, O-O) and H_2O (O-H stretch, H-O-H bend). For the self-reaction of CH_3O_2 and the cross-reaction of CH_3O_2 + HO_2, we therefore would not expect rate enhancement from the water complex with CH_3O_2.

Kinetic studies on the cross-reaction between HO_2 and CH_3O_2 radicals indicate that the reaction rate constant is not enhanced by water vapor under the conditions probed. In this work, the cross-reaction has 7- 15 % of the HO_2 complexed with water. We should be able to see an enhancement since the water is strongly bound to the HO_2 and because the water can mode match with HO_2. However, inefficient coupling occurs because of the steric hindrance from the methyl group. The water is distanced from the HO_2 such that it cannot efficiently transfer energy from the O-H stretch occurring as the activated complex is forming. Figures 15 and 16 show the calculated PES by Clark et al. of the cross-reaction with and without the HO_2-H_2O complex.

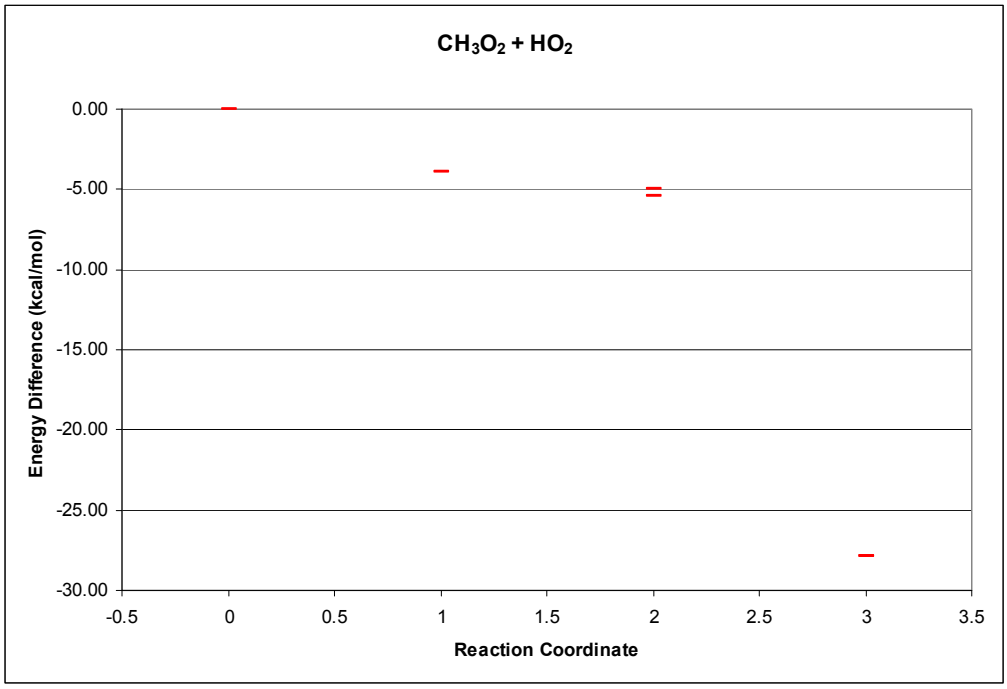

Figure 15 Potential energy surface of CH_3O_2 + HO_2 as calculated by Clark et al.

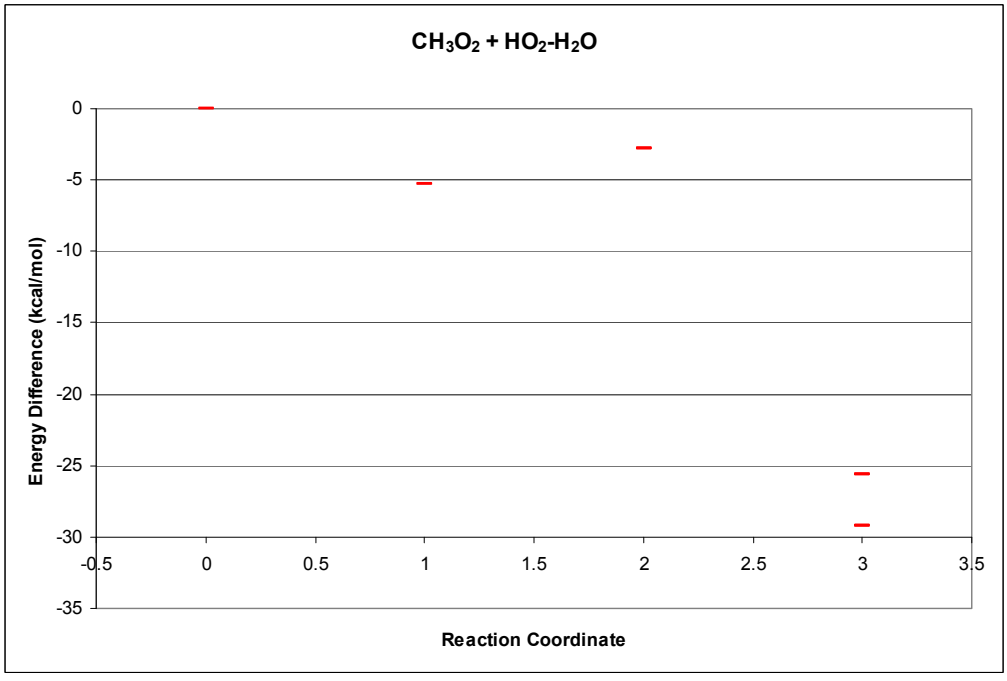

Figure 16 Potential energy surface of CH_3O_2 + HO_2–H_2O as calculated by Clark et al.

Studying other carbonyl and alcohol moieties of peroxy radicals, which Clark et al. has shown to have stronger binding energies, may show rate enhancements due to the formation of a water complex along with efficient coupling.

While the presence of water needs to be accounted for in HO_2 atmospheric chemistry, the effect on CH_3O_2 is small at best. Modeling provides information on many types of pollution and its sources (i.e., O_3 production, acid rain). Understanding the changes water causes in rate constants for other RO_2 chemistry will lead to more accurate modeling and a better understanding of the complexity of the atmosphere.

REFERENCES

(1) Finalyson-Pitts, B.J; Pitts, J.N., Jr. *Atmospheric Chemistry*; Wiley: New York, 1986.

(2) Kircher, C.C.; Sander, S.P. *J. Phys. Chem.* **1984**, *88*, 2082-2091.

(3) Sander, S.P.; Peterson, M.; Watson, R.T. J.Phys. Chem. **1982**, *86*, 1236-1240.

(4) Kanno, N.; Tonokura, K.; Tezaki, A.; Koshi, M. *J. Phys. Chem. A* **2005**, *109*, 3153-3158.

(5) Maricq, M.M.; Szente, J.J. *J. Phys. Chem.* **1994**, *98*, 2078-2082.

(6) Christensen, L.E.; Hansen, J.C.; Francisco, J.S.; Sander, S.P.; Okumura, M. *J. Phys. Chem. A* **2006**, *110*, 6948-6959.

(7) Stockwell, W.R. *J. Geo. Res.* **1995**, *110*, 11695-11698.

(8) Suma, K.; Sumiyoshi, Y.; Endo, Y. *Science* **2006**, *311*, 1278-1281.

(9) Aloisio, S.; Francisco, J.S. *J. Phys. Chem. A* **1998**, *102*, 1899-1902.

(10) Atkinson, R.; Baulch, D.L.; Cox, R.A.; Hampson, R.F., Jr.; Kerr, J.A.; Rossi, M.J.; Troe, J. *J. Phys. Chem. Ref. Data*, **1997**, *26*, 521.

(11) Clark, J.; English, A.M.; Hansen, J.C.; Francisco, J.S. *J. Phys. Chem. A* **2007**, in press.

(12) DeMore, W.B.; Sander, S.P.; Golden, D.M.; Hampson, R.F.; Kurylo, M.J.; Howard, C.J.; Ravishankara, A.R.; Kolb, C.E.; Molina, M.J., Chemical Kinetics and Photochemical Data for Use in Stratospheric Modeling. Evaluation #12, *JPL Publ.* **1997**, *4*, JPL: Pasadena, California, 1997.

(13) Bryukov, M.G.; Dellinger, B.; Knyazev, V.P., *J. Phys. Chem. A*, **2006**, *110*, 936-943.

(14) Atkinson, R.; Baulch, D.L.; Cox, R.A.; Crowley, J.N.; Hampson, R.F, Jr.; Kerr, J.A.; Rossi, M.J.; Troe, J. *IUPAC Subcommittee on Gas Kinetic Data Evaluation for Atmospheric ChemistryWeb Version*, **2001**, *Dec*, 1-56.

(15) Maricq, M.M.; Szente, J.J.; Kaiser, E.W.; Shi, J. *J. Phys. Chem*. **1994**, *98*, 2083-2089.

(16) Timonen, R. *Ann. Acad. Sci. Fenn. Ser. A2* **1988**, *218*, 5-45.

(17) Timonen, R.; Kalliorinne, K.; Koskikallio, *J. Acta. Chem. Scand. Ser. A* **1986**, *40*, 459-466.

(18) Baulch, D.L.; Cobos, C.J.; Cox, R.A.; Frank, P.; Hayman, G.; Just, Th.; Kerr, J.A.; Murrells, T.; Pilling, M.J.; Troe, J.; Walker, R.W.; Warnatz, J. *J. Phys. Chem. Ref. Data* **1994**, *23 (Suppl. 1)*, 847.

(19) Hassinen, E.; Koskikallio, J. *Acta. Chem. Scand. Ser. A* **1979**, *33*, 625.

(20) Heicklen, J. *Adv. Photochem.*, **1988**, *14*, 177.

(21) Cattell, F.C.; Cox, R.A. *J. Chem. Soc. Faraday Trans. 2* **1986**, *82*, 1413

(22) Biggs, P.; Canosa-Mas, C.E.; Fracheboud, J-M.; Marston, G.; Shallcross, D.E.; Wayne, R.P. *J. Chem. Soc. Faraday Trans.*, **1995**, *91*, 3045-3053.

(23) Butler, J.F.; Calawa, A.R.; Phelan, Jr., R.J.; Harman, T.C.; Strauss, A.J.; Rediker, R.H. *Appl. Phys. Lett.* **1964**, *5*, 75.

(24) Maricq, M.M.; Wallington, T.J. *J. Phys. Chem.* **1992**, *96*, 986-992.